Supporting Information

Octave-Spanning Broadband Absorption of Terahertz Light using Metasurface Fractal-Cross Absorbers

Mitchell Kenney, James Grant, Yash D. Shah, Ivonne Escorcia-Carranza, Mark Humphreys, David R. S. Cumming

School of Engineering, University of Glasgow, G12 8LT, UK

Contents:

Supporting Note 1: Dielectric thickness dependency of absorption spectra

It is well known that optimisation of the dielectric spacer thickness between the ground-plane and resonant array is required for the desired absorption characteristics of a metal-insulator-metal (MIM) perfect absorber. We carried out computer simulations using the commercially available software CST Microwave Studio, for a range of dielectric spacer thicknesses. In the simulation, we used polyimide (PI2545) as the dielectric spacer, with preliminary refractive index values of $n = 1.68 + 0.06i$ [1,2] and for the gold ground-plane and fractal cross absorbers we used a conductivity of $\sigma = 4 \times 10^7$ Sm^{-1} [1,2]. Polyimide thicknesses were swept from 3 μm up to 13 μm in steps of 0.5 μm. The light was normally incident.

Shown in Fig. S1 are the results for fractal levels 1-3 and polyimide only. Figs. S1a-c correspond to the level 1 fractal, with Figs. S1c-f corresponding to the level 2 fractal, Figs. S1g-i corresponding to the level 3 fractal, and Figs. S1j-l corresponding to polyimide only without any fractal structures. Due to the large number of spectra obtained for each design, the corresponding results were split up onto 3 plots, with plots on the *left* (a,d,g,j) spanning 3 – 6 μm, plots in the *middle* (b,e,h,k) spanning 6.5 – 9.5 μm, and plots on the *right* (c,f,i,l) spanning 10 – 13 μm. A typical trend is seen for all spectra (excluding polyimide-only) on the left, with each design portraying narrowband and high absorption response. Similarly, for all

spectra on the right, a broadband trend occurs for all designs, owing to the superposition of the polyimide absorption (shown in Fig. S1l) with the fractal cross responses. This is evidenced by the plots shown in the middle of Fig. S1, in between the narrowband and broadband regimes; as the polyimide thickness increases, we start to see a second peak (for level 1-3 fractal plots) moving from higher to lower frequencies. This second peak is attributed to anti-reflection coating (ARC) type absorption in the polyimide layer. As seen in Fig. S1k, the absorption response for polyimide-only starts to come into play, and therefore modifies the spectral

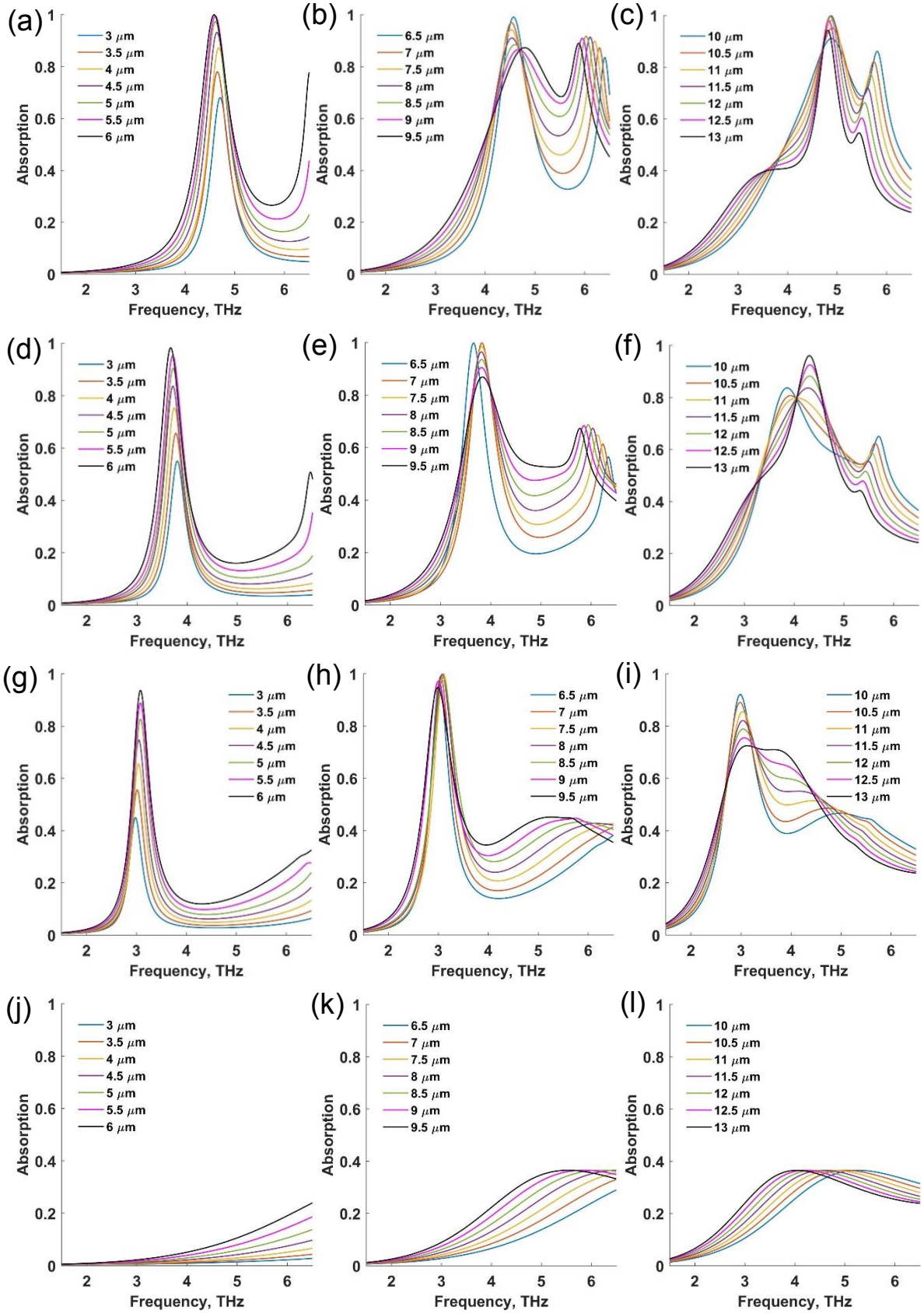

Figure S1 – Numerically simulated absorption response for different fractal designs when polyimide thickness varies. Each row corresponds to a different design, where **(a-c)** corresponds to the level 1 fractal, **(d-f)** to the level 2 fractal, **(g-i)** to the level 3 fractal, and **(j-k)** for the polyimide-only case without any fractal cross structures. The polyimide thickness is swept from 3 µm to 13 µm in steps of 0.5 µm, with seven spectra shown per plot for better analysis by the reader.

responses of the fractal cross designs. We therefore postulate that the absorption which takes place within the polyimide layer itself it critical to obtaining broadband absorption.

As seen in the main article, we find that when combining all fractal levels into a supercell arrangement, we can obtain a broadband absorption response covering the combined corresponding frequencies for each fractal level. However, for thin polyimide samples (5 μm, Fig. 2e) a limited absorption efficiency is witnessed, whilst thick polyimide (11 μm, Fig. 2f) provides much improved absorption enhancement. Shown below in Fig. S2 are the broadband spectral responses of the supercell configuration. We clearly see that for thin samples (Fig. S2,a), the absorption efficiency is very diminished, whilst thicker samples (Fig. S2,c) show a distinct increase in absorption magnitude. We choose 11μm for the main text designs as it has the best trade-off between absorption magnitude and broad bandwidth for our designs. An explanation behind the thicker polyimide giving a better response is given in Supplementary note 4.

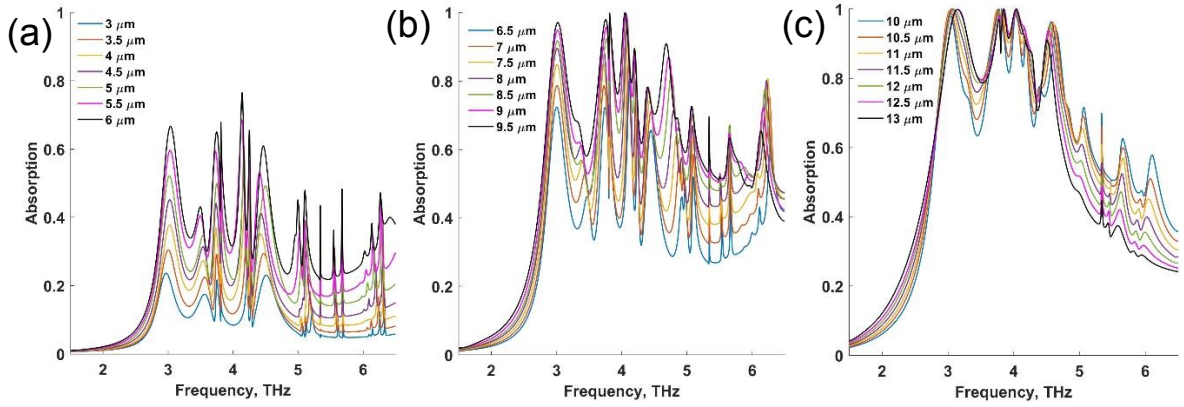

Figure S2 - Numerically simulated absorption response for varying polyimide thickness of the broadband supercell fractal design. The polyimide thickness was swept from 3 μm to 13 μm, in steps of 0.5 μm, and is separated into 3 plots for ease of viewing. **(a)** Spectral responses for 3 – 6 μm polyimide thicknesses. **(b)** Spectral responses for 6.5 – 9.5 μm polyimide thicknesses. **(c)** Spectral responses for 10 – 13 μm polyimide thicknesses. It is clear that only the spectra shown in (c) have sufficiently high broadband absorption, whilst the thinner polyimide thickness samples have diminished absorption performance. This is attributed to the thinner samples relying on induced ground-plane currents being out of phase for each fractal cross, and therefore coherence is broken resulting in poor overall absorption. The thicker samples rely on Salisbury Screen and anti-reflection coating type absorption of the polyimide, resulting in much higher absorption.

Supplementary Note 2: Average absorption of simulated broadband spectra

An ideal situation for a broadband absorber would be for the presence of a flat response over the peak absorption. However, this is not truly realistic, due to the individual crosses resulting in higher absorptions at their corresponding resonance frequencies within the broadband spectrum. Because of this, it therefore makes sense to calculate an *average* peak absorption, taking into account the absorption minima and maxima over the bandwidth. An ideal method for this would be to integrate over the curve. However, both numerically simulated and experimentally obtained results have curves fitted to discrete data points. Therefore, we instead sum up the values of the data points, and divide this by the total number of points in a specific range.

In order to choose the correct spectral bandwidth (frequency range) over which to average the peak absorption, we must define the minimum absorption value present within the spectrum. Shown in Fig. S3 is the numerically simulated spectrum for the broadband supercell design on 11 μm thick polyimide. The minima occurring within the broad bandwidth occurs at 3.42 THz, with an absorption magnitude of 69.92 %. We choose this as our baseline, and then match the corresponding minimum and maximum frequency values at which this absorption magnitude also occurs; these happen to be 2.8 THz and 4.819 THz, as shown in Fig. S3. Using these minimum and maximum frequencies, we then find the average absorption of the curve above the red dashed line, which is equivalent to finding the height of a rectangle with an area equal

to the shaded blue area of Fig. S3, and length $\Delta f = 4.819\ \text{THz} - 2.8\ \text{THz} = 2.019\ \text{THz}$. Due to the curve in S3 being composed from discretely simulated data points, we used Matlab to assist in the calculation. Data files were exported from CST Microwave Studio, composed of 1001x2 data points, with the first column attributed to the frequency value, and the second column attributed to its corresponding absorption value. Data point #1 and #1001 corresponded to the

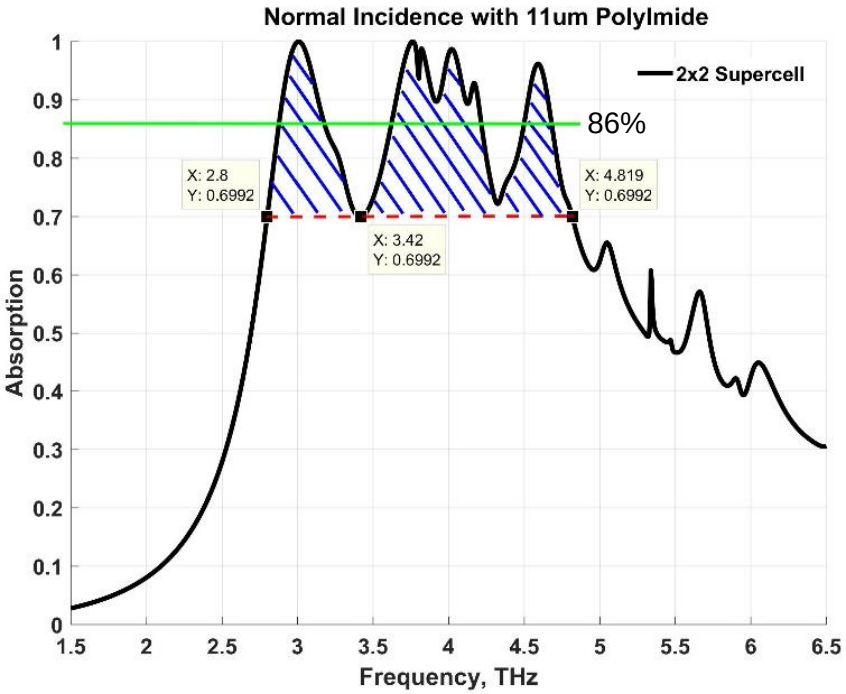

Figure S3 - Averaging of the peak absorption for the numerically simulated broadband supercell absorber. The red dashed line indicates the equi-absorption value to match up the minimum and maximum bandwidth frequencies for the dip occurring at 3.42 THz. The minima corresponds to 2.8 THz, whilst the maxima is 4.819 THz. The blue shaded region above the red dashed line is then the area considered for averaging, akin to integration. The average value is found by summing of the absorption values of each point of the curve surrounding the shaded region, and dividing by the total number of data points over this region. The green line indicates the averaged value of 86 %.

min. and max. frequency limits of the simulation (1.5 THz and 7 THz, respectively), with data points in between linearly increasing in frequency. For calculating the average absorption, S, with these data points, we used equation given below:

$$S = \left(\sum_{n=a}^{b} A(n)\right) \Big/ [(b-a)+1]$$

where a and b correspond to the minimum and maximum data point number (where $a = \#237$ corresponds to the minimum frequency value of 2.8 THz, and $b = \#605$ corresponds to the maximum frequency value of 4.819 THz), and $A(n)$ is the absorption value at the data point n. Using this equation, we obtain an average absorption of $S = 85.9$ %, which we round up to 86 % as indicated by the green line in Fig. S3.

Supplementary Note 3: Experimental results for 5.59 µm polyimide samples

The experimentally obtained spectra for the narrowband devices, fabricated on 5.59 µm PI, are shown in Fig. S4. It is clear that they have very similar spectra when compared to the simulations shown in Fig. 2a of the main manuscript. Experimental resonance frequencies (from lowest to highest) occur at 2.98 THz, 3.62 THz, and 4.25 THz, for fractal levels 3, 2, and 1 respectively. These frequencies differ slightly from the simulated values of 3.08 THz (level 3), 3.72 THz (level 2), and 4.61 THz (level 1) due to uniformity of polyimide thickness, refractive index values used in simulation, fabrication errors, and that experimental results were carried out at 30° incidence compared to normal incidence in the simulations. The absorption efficiencies are still very high, however, where fractal levels 3, 2 and 1 have corresponding peak absorption values of 82 %, 90 %, and 86 % respectively. A slight kink occurs in all spectra at ~ 4.75 THz, which is attributed to the absorption spectra of the polyimide layer alone, shown as the dashed magenta curve in Fig. S4a, where absorption in the polyimide layer will be additive to the spectra of the metasurface absorption as measured by the FTIR.

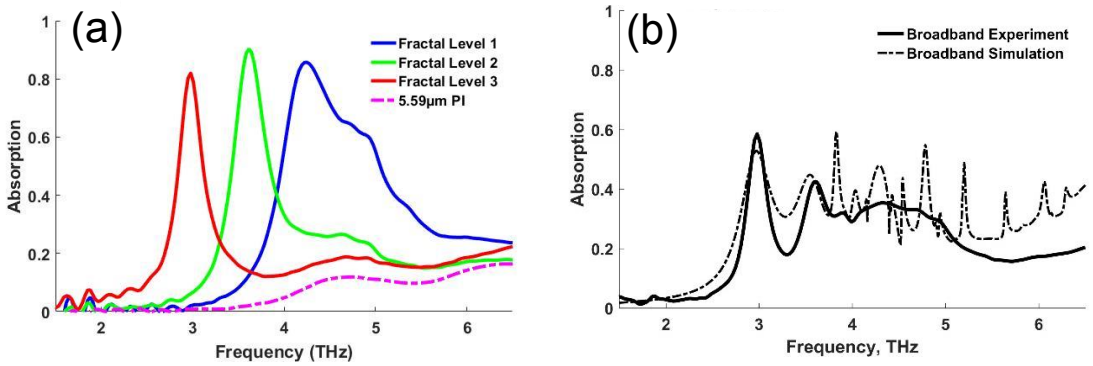

Figure S4 – Experimental and Modified Simulation results. Experimentally obtained FTIR spectra carried out at 30° incidence, and matched simulation. **(a)** FTIR spectra for the single-band fractal designs, using **a** 5.59 µm thick polyimide interlayer. The magenta dashed lines are the result of polyimide (PI) only with no fractal cross structures. **(b)** Broadband spectra for the supercell design on 5.59 µm polyimide thickness. Solid lines are the experimentally obtained FTIR spectra, whilst dashed lines are the matched simulation results. The simulation was also carried out at an incident angle of 30°.

The supercell arrangement shows good experimental agreement (Fig. S4b) with the preliminary simulations (Fig. 2e), in that lessened broadband absorption takes place. This is attributed to the out-of-phase ground-plane surface currents for each fractal cross. The simulated curve shown in Fig. S4b uses a modified refractive index of n = 1.71 + 0.08i. This modified refractive index was obtained through fitting of the simulated broadband supercell design to the experimental result for 11.24 μm polyimide, given in Fig. 3d in the main text. The simulation was carried out at 30° oblique incidence, and shows a good correspondence to the experimental results with a noticeably good matching of the peak at ~ 3 THz.

Supplementary Note 4: Simulated spectra for single-band absorbers matched to FTIR results

Using the broadband experimental result seen in Fig. 3d (main text) as a basis for fitting, the simulated curve in Fig. 3d was obtained by using a refractive index of n = 1.71 + 0.08i. Because the polyimide is considered to be dispersive with wavelength, the fitted refractive index is not considered to be truly accurate. However, a good comparison can be seen between the experimental and simulated curves. Using this refractive index, we obtained numerically simulated curves for the single-band designs using the individual fractal crosses. These results are shown below in Fig. S5, along with the experimentally obtained FTIR results. For the narrowband designs, shown in Fig. S5a, using 5.59 μm thick polyimide, both FTIR (solid lines) and simulated (dashed lines) spectra show very good agreement. Only the level 1 fractal design shows a slight disagreement due to the presence of the kink for the FTIR spectrum, owing to the absorption in polyimide. The sharp spikes present in the simulated spectra are assumed to

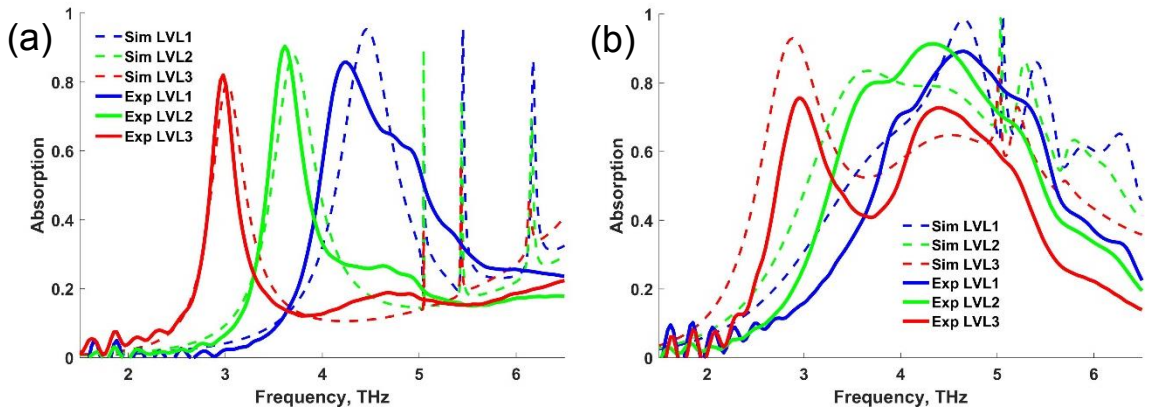

Figure S5 - Experimentally obtained and matched numerically simulated spectra for individual fractal designs. The plots show the spectra obtained experimentally from FTIR (solid lines) and the corresponding matched simulation results (dashed lines), for **(a)** 5.59 µm, and **(b)** 11.24 µm thick polyimide samples.

be artefacts caused by the limited meshing of the design and also due to the incident oblique angle being 30°, as none of these features appear in the experimentally obtained FTIR results. Results for the thicker polyimide of 11.24µm thickness, used for the broadband individual cross designs, are given in Fig. S5b. Although the simulated curves do not match well with FTIR results, a general trend exists for the prominent features. As mentioned in the main article, the level 3 fractal cross (red curves) has two peaks, which we attribute to be due to two different absorption mechanisms; this trend is also seen in the simulated results, with the peaks situated at very similar frequencies for both FTIR and simulated spectra. Again, the spurious peaks in Fig. S5b are attributed to be due to numerical meshing limitations and oblique incidence, as they do not appear in experimentally obtained spectra.

Supplementary Note 5: Theoretical postulation for two-mechanism absorption in thick absorber designs

Here, we postulate the difference in absorption mechanisms for thin and thick polyimide thicknesses, which can be general for lossy dielectric spacers. First, we consider the case of thick polyimide, for the experimentally obtained spectra of the level 3 fractal design (red curve, Fig. 3a in main text), showing two distinct absorption peaks at 2.95 THz and ~4.5 THz. For anti-reflection coating (ARC) type phenomena to take place, the necessary condition for

absorption is that the polyimide thickness corresponds to $\lambda/4$, such that a π phase difference between the light reflected off the air/polyimide and polyimide/ground-plane boundaries results in destructive interference. Assuming a refractive index of polyimide as n = 1.71, and the ARC Fabry-Pérot type resonance taking place at ~ 4.5 THz (= 67 μm), we calculate the wavelength within the PI layer as $\lambda = \lambda_0/n$ = 39.0 μm. The polyimide thickness of 11.24 μm is therefore approximately equivalent to $\lambda/4$ at this resonance wavelength. However, the refractive index of the polyimide is not considered to be accurate, due to dispersion, and multi-reflections will contribute to the absorption frequency. For Salisbury Screen type operation at 2.95 THz it is assumed that the presence of the fractal crosses will significantly modify the complex transmission and reflection coefficients of light from either side (either air-to-polyimide or polyimide-to-air directions). This will in turn result in the phases of the transmitted and reflected light being different to that for the ARC case, due to the highly resonant nature of the metal crosses, therefore explaining the resonance frequency disparity. The presence of resonant structures is explained in Ref. [[3]], which produce a significant phase modification to the transmitted and reflected light.

Next, we look at the thin polyimide case, and why the supercell broadband efficiency is so diminished compared to single-band designs. Shown in Fig. S6 are 2D current density plots showing the current flow for all four designs (level 1, 2, 3 fractals, and supercell designs). The single-band designs are given in the left column of Fig. S5 (Fig. S5a,c,e correspond to fractal levels 1, 2, 3, respectively). For each corresponding single band design, we choose the resonance frequencies of each fractal level (shown in Fig. 2a of the main text), and assign a current density field monitor in CST MWS. The resonance frequencies, and therefore corresponding current density plots, for fractal levels 1, 2, 3 are at 4.61 THz, 3.72 THz, 3.08 THz, respectively. It is clear for all single-band absorbers (left column of Fig. S5) that at their resonant frequencies strong opposite current flows on the cross and ground-plane occur. This

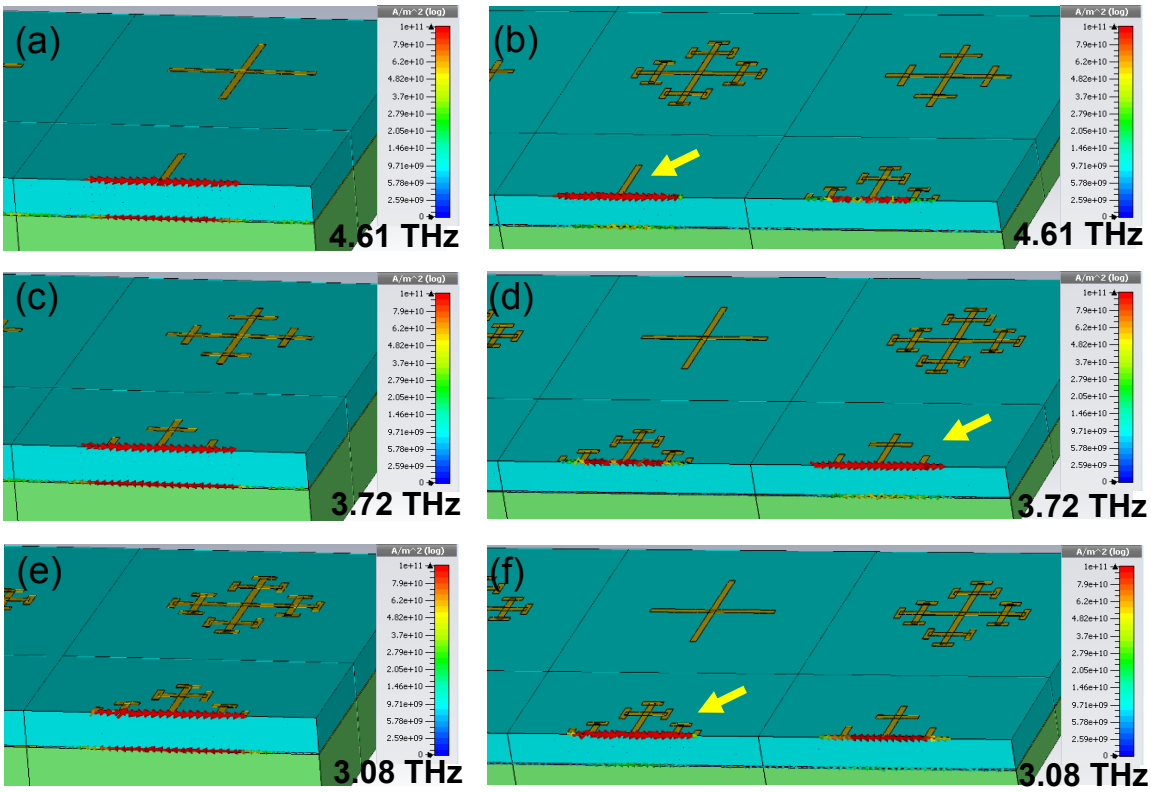

Figure S6 – 2D Current Density maps showing current flow of each fractal cross on 5µm polyimide. Left column (a, c, e) corresponding to single-band designs, whilst the right column (b, d, f) are their corresponding broadband responses. **(a,b)** the level 1 fractal cross current density plots for single-band (a) and broad-band designs (b) at the resonance frequency of 4.61 THz. **(c,d)** the level 2 fractal cross current density plots for single-band (a) and broad-band designs (b) at the resonance frequency of 3.72 THz. **(e,f)** the level 3 fractal cross current density plots for single-band (a) and broad-band designs (b) at the resonance frequency of 3.08 THz. All current density plots were normalised to the same intensity, shown in the bar to the right of each figure, to give a comparable indication of currents. The yellow arrows in the broadband current density plots point to the resonant cross in question.

is in agreement with the standard metamaterial absorber explanation, where the opposite current flows result in an induced magnetic dipole within the dielectric, which therefore modifies the effective magnetic permeability. However, once we combine the three fractal level into the supercell design (Fig. 1d of main text), such coherent magnetic resonances no longer occur. In the right column of Fig. S6 are the current density plots for the supercell design, at the corresponding resonant frequencies given in the left column (for single-band designs). The yellow arrows point out the fractal cross in question at each frequency. It is clear that current flow on the ground-plane no longer occurs at the resonance frequencies for the broadband design, as it does for the single-band designs. We attribute this to the anti-currents of the surrounding fractal crosses, which are out of phase with the resonant cross at its resonance frequency. This is especially visible in Figs. S6d and f, where the current flow on the

surrounding crosses are the opposite directions to the resonance cross in question. This in turn results in a π phase difference in the ground-plane currents, and can therefore destructively interfere. This breaks the coherent resonance effect of the single-band absorbers, leading to imperfect resonance conditions, and a difference in the effective magnetic permeability, ultimately changing the effective impedance of the broadband devices.

Supplementary Note 6: Equivalence of fractals and scaled-cross supercells

As was explained for Fig. 1c of the main manuscript, fractal crosses of level 2 and level 3 are equivalent in resonance frequency as simple scaled-up crosses with size increases (from the original size of 20 μm) of ~25% and ~50%, respectively. Due to this, it is interesting to see the situation where we instead replace the fractal crosses for these scaled simple crosses in a supercell arrangement, and try to replicate the broadband response we obtained from the case for 11.24 μm polyimide (as given for the more accurately matched simulation in Fig. 3d).

Shown below in Figure S7 are the results for this. Figure S7a and S7b are the designs for the fractal and scaled simple-cross supercells, respectively, where the replaced simple crosses have equivalent absorption frequencies as their fractal counterparts. Using the same polyimide permittivity parameters of $n = 1.71 + 0.08i$, thickness of 11.24 μm, and incident angle of 30° we obtained the simple-cross supercell spectra given in Fig. S7c (orange curve). It is very comparable to the fractal supercell result (blue curve) in terms of peak absorption at the different peaks and broad bandwidth. However, the simple cross design shows a much higher average peak bandwidth with much smaller minima occurring. We attribute this to the introduction of much stronger coupling between crosses compared to the fractal case. In order to confirm this, we ran 2D electric field profile simulations at 4 THz, given in Fig. S7d,e. We see, as expected, in Fig. S7d that the fractal crosses have very minimal coupling, due to their compact

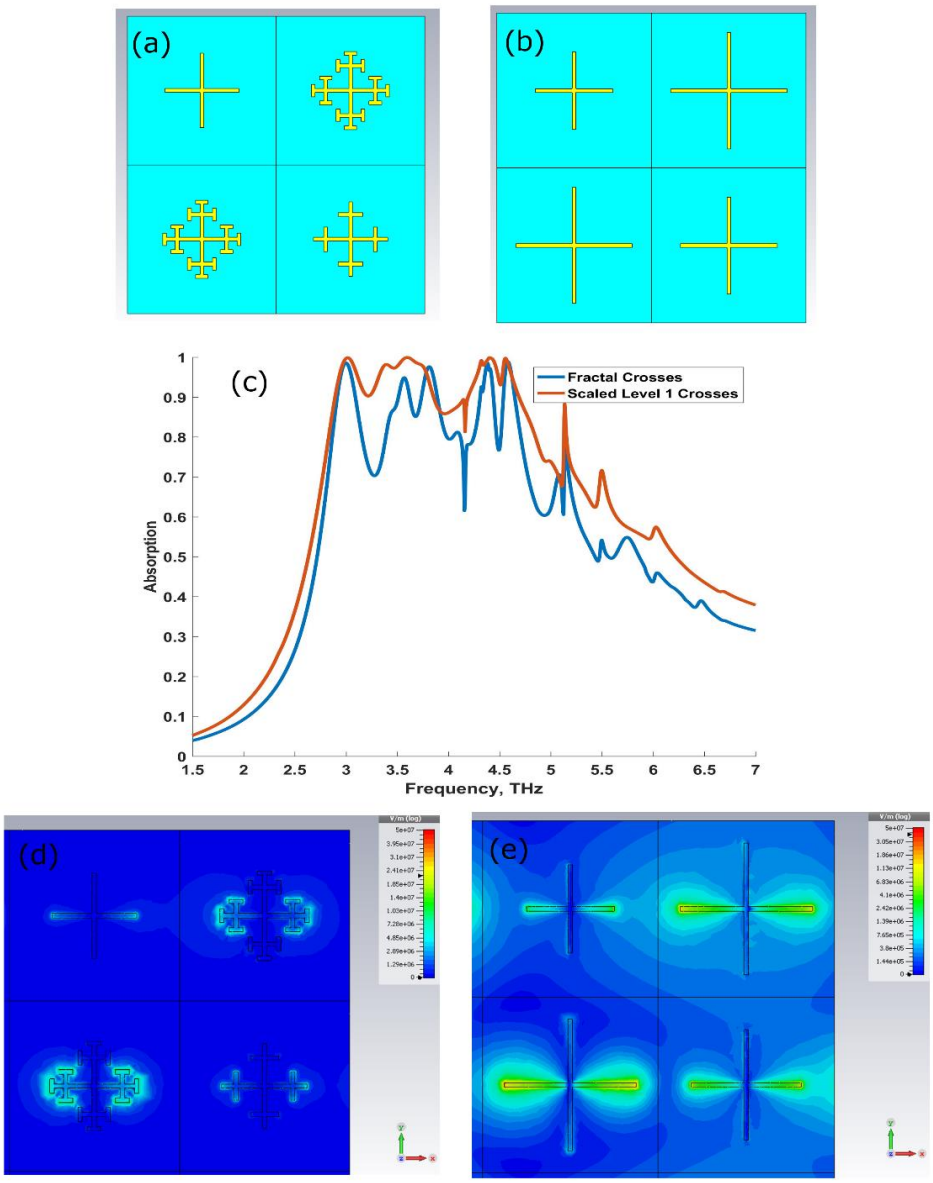

Figure S7 – Comparison of using fractal supercells and scaled simple-cross supercells

(a) Our original fractal cross supercell design, compared to the equivalent **(b)** scaled simple-cross supercell design, where the scaled crosses replacing fractal cross levels 2 and 3 have the same resonant frequencies. **(c)** both fractal supercell (blue) and scaled cross supercell (orange) spectra. **(d)** 2D electric field profiles for the fractal supercell design, and **(e)** scaled cross supercell design. The scale bar is logarithmic and 5e7 V/m for both profiles, showing that the simple crosses have much stronger coupling.

size compared to the unit cell size (~half the length of the unit cell). For the simple-crosses, we see that coupling is much more pronounced. This is due to the fact that the longer arms mean there is a smaller cross-to-cross distance and so dipolar resonances will be coupled. Such a coupling effect will result in hybridized resonant responses, which will modify the effective capacitances and inductances. If coupling is not a concern to the reader, then it would be beneficial to use the standard scaled simple crosses to maximise absorption. However, we used

fractal crosses for the case where individual absorption responses may be required in an application, such as bolometric sensing, as the crosses are not strongly coupled, and remain very subwavelength.

Supplementary Note 7: Average absorption of experimental broadband spectra

Similar to the case in Supplementary Note 2, we have now the experimentally obtained FTIR broadband spectra from the supercell fractal design atop 11.24 μm thick polyimide. The differences between the simulation results in Supplementary Note 2 (and Fig. 2f of the main text) and the experimentally obtained results here (and Fig. 3d of the main text) are that the experiment has light incident at 30°, whilst for the simulation it is normal incidence, and the fabricated polyimide thickness is 11.24 μm as opposed to 11 μm for simulation. The experimentally obtained FTIR spectrum for the broadband device is given in Fig. S8. These

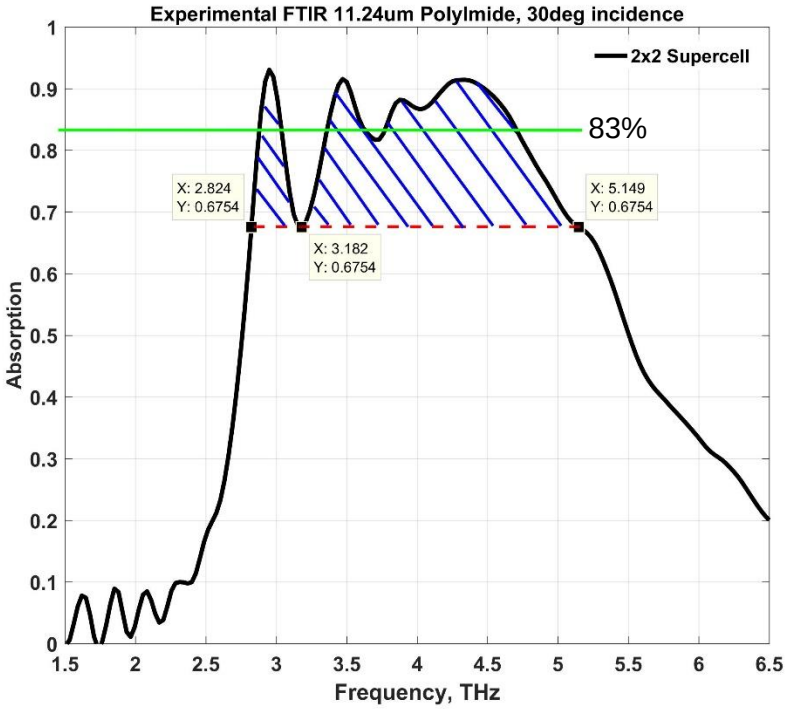

Figure S8 - Averaging of the peak absorption for the experimental FTIR broadband spectrum. The red dashed line indicates the equi-absorption value to match up the minimum and maximum bandwidth frequencies for the dip occurring at 3.182 THz. The minima corresponds to 2.824 THz, whilst the maxima is 5.149 THz. The blue shaded region above the red dashed line is then the area considered for averaging, akin to integration. The average value is found by summing of the absorption values of each point of the curve surrounding the shaded region, and dividing by the total number of data points over this region. The green line indicates the averaged value of 83 %.

differences, as well as the assumed refractive index of polyimide for polyimide lead to differences in absorption bandwidth and magnitude. As such, we suggest a reliable figure of merit by calculating the *average p*eak absorption by integrating the curve above the absorption dip/minima occurring in the broadband region, and dividing by the bandwidth at the equi-absorption line. Using the absorption dip at 3.182 THz, we have a value of 67.54%. The equi-absorption line then gives us a frequency bandwidth between the minimum (at 2.82 THz) and maximum (5.149 THz) frequency values. Again, because the experimentally obtained data curve is composed of a finite number of data points, we use the formula given in supplementary note 2, where data point number (#) $a = \#445$ and $b = \#525$. The average absorption value of the curve above the red-dashed line (Fig. S8) is calculated to be $S = 82.9$ %, which we round up to 83 % as indicated by the solid green line in Fig. S8.

Supplementary Note 8: 2D electric field profiles of simulated supercell design

In order to further analyse experimental results, we performed a series of numerical simulations, using both CST MWS and Lumerical softwares. To examine the broadband characteristics of the supercell design (11.24 μm polyimide), the five prominent peaks of the matched simulation spectra were investigated using 2D electric field monitors. **Figure S9**a shows a zoomed in view of the spectra originally given in Figure 3d to clearly show the reader the positions of each peak. The five peaks are referred to as I-V, corresponding to **Figures S9b-f**, respectively. The frequency of each peak (I-V) is given in white text inset at the bottom-left of each electric field profile in Figures S9b-f. All electric field profiles were normalised to the same scale in order to provide a direct comparison between resonance strengths. As a note, there appears to be a sharp dip at a frequency of ~ 4.16 THz (72 μm) in the simulation spectra in Figure S9a. We attribute this to be related to a Wood's Anomaly (WA),[4,5] typically at a wavelength of the order of $\lambda_{WA} = n \cdot P$, where n is the refractive index of the substrate and P

is the periodicity of the resonant structures. In our case, $n \approx 1.71$ and $P = 40\ \mu m$, giving a Wood's Anomaly wavelength of $\lambda_{WA} \approx 68\ \mu m$, very close to the spectral dip of 72 μm.

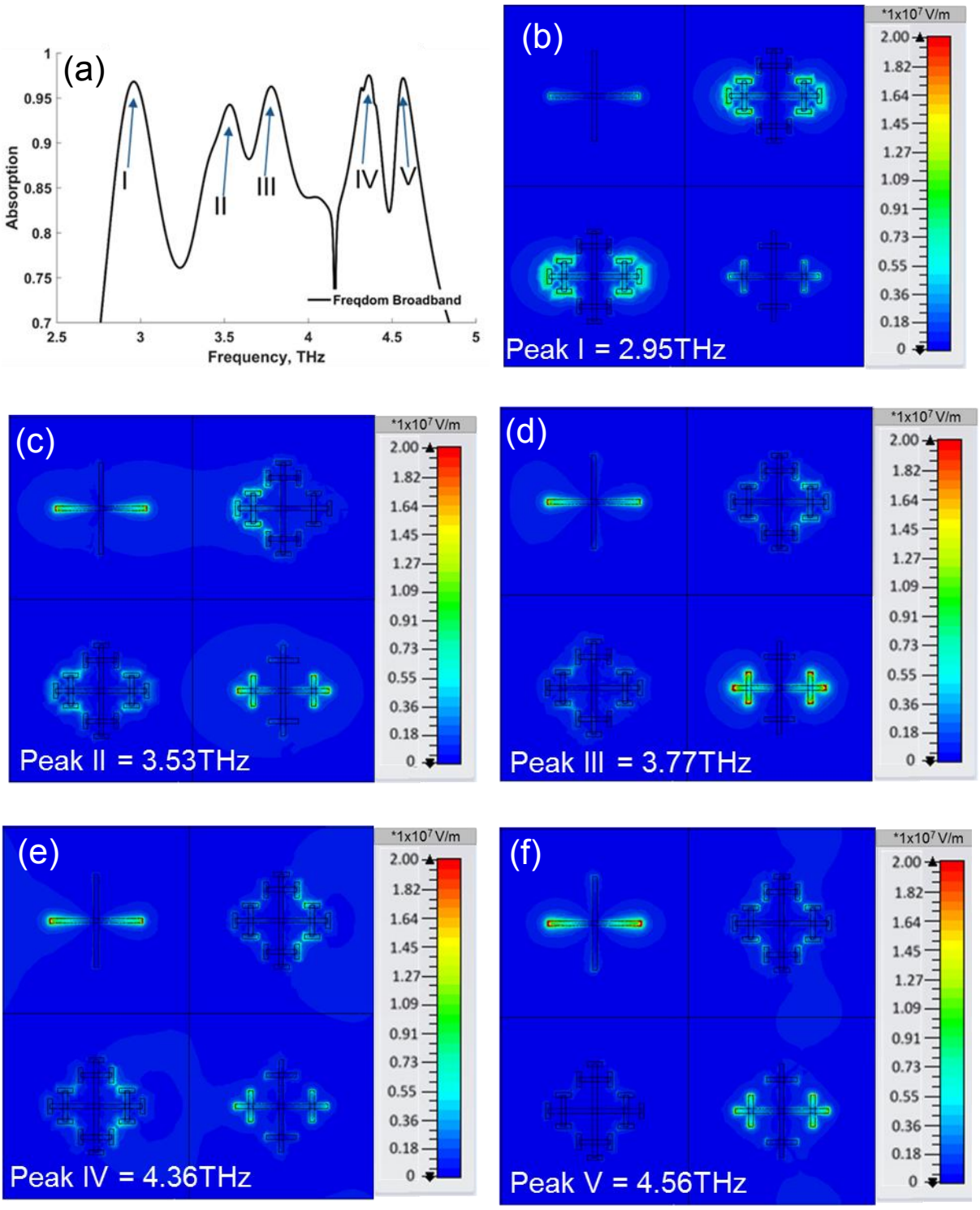

Figure S9 – Numerical E-Field profiles for broadband peaks. (a) Zoomed in simulated spectra, given in Fig. 4d, showing the five peaks. Peaks (**I-V**) correspond to figs **(b-f)**, the simulated 2D electric field profiles of a broadband supercell with a beam incident at an angle of 30°. The sharp dip in **(a)** at ~ 4.16 THz is attributed to a Wood's anomaly.

In Figure S9b it can be seen that for peak '**I**' (2.95 THz) the primary dipolar response is that of the level 3 fractal, in good agreement with the resonance frequency of the single-band level 3 fractal in Figure 4b occurring at 2.95 THz. The electric responses of level 1 and 2 fractal crosses are diminished and therefore do not strongly contribute to the absorption taking place for this peak. Similarly for peak '**III**' (Figure S9d), the level 2 fractal resonance solely appears to dominate at 3.77 THz. This is also true for peak '**V**' absorbing at 4.56 THz (Figure S9f) where the level 1 fractal shows the strongest resonant response. Fractal levels 1, 2 and 3 are therefore independently attributed to the large absorption peaks labelled as '**I**', '**III**', and '**V**', respectively. For Figures S9c and S9e, the electric field responses are more complex, with no clear fractal being dominant. The peaks '**II**' and '**IV**' are therefore assumed to be due to hybridisation and superpositions between the aforementioned resonances. One interesting result is the asymmetric electric field distribution for the level 3 fractals in Figures S9c and S9e. This is attributed to the light incidence being 30°, and therefore reaching different parts of the 'supercell' with different phases. Due to the relatively large distance between crosses (40 μm) the dipolar coupling of electric fields is negligible. This is advantageous for design, as coupling would introduce nonlinearities into the functionality of a broadband absorber.

Supplementary Note 9 – Simulated angular dependence of 5.59 μm polyimide samples

The angular dependence of 5.59 μm thickness polyimide (narrow-band) samples were simulated using Lumerical FDTD software. The oblique angle was varied between 0 and 45, for the four fractal designs: single-band absorbers (fractal levels 1-3); and broadband supercell absorber. The results are shown in Figure S10. All plots show distinctly narrow-band absorption, as supported by simulation and experimental results. The angular dependence seems to have little effect, with narrowband absorption for all designs occurring over a large angular range. Above 30°, there seems to be a slight shift of the resonance for the level 1 fractal design in Figure S10a, which is attributed to the presence of the secondary absorption curve

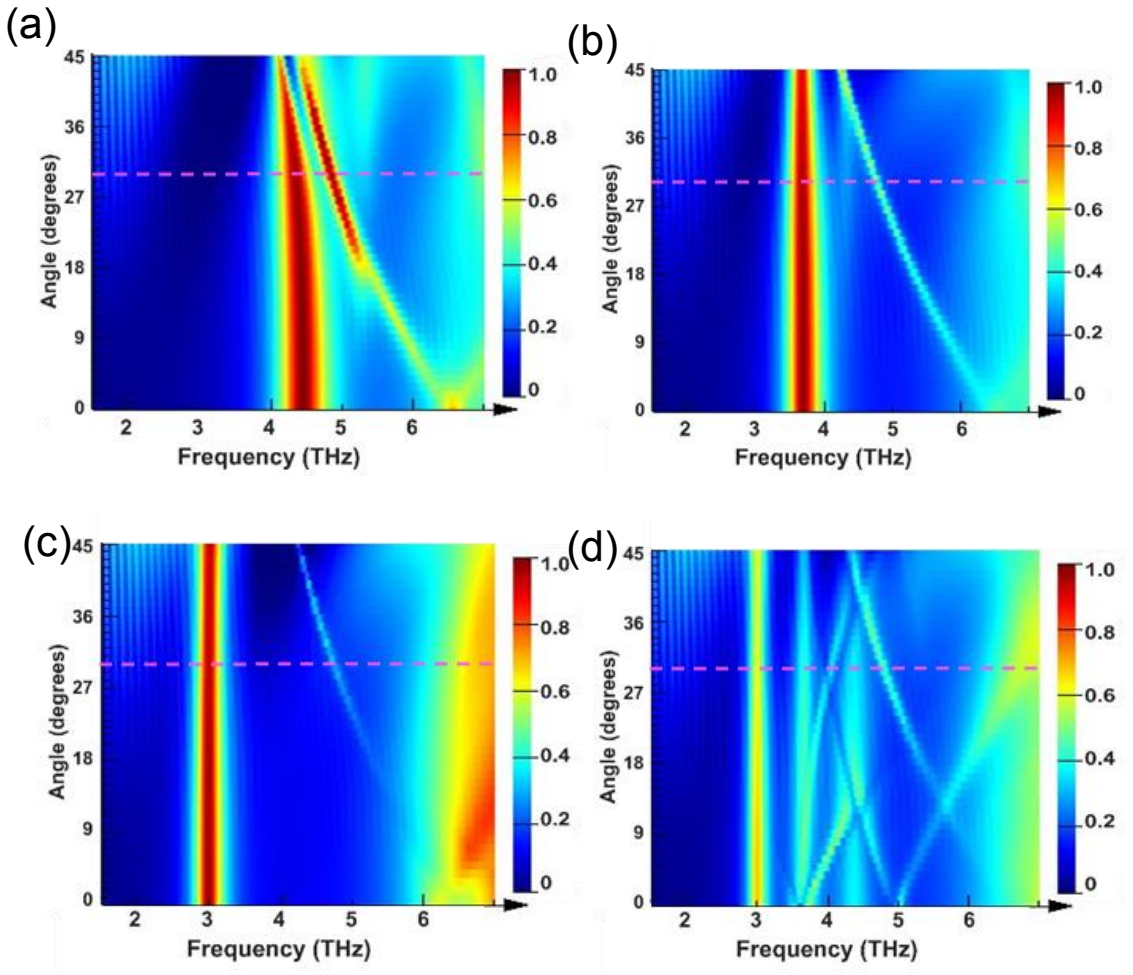

Figure S10 – Numerically simulated maps of angle-dependent absorption response. Numerical simulations of the fractal cross absorbers were performed using Lumerical FDTD where the oblique angle of incidence was varied between 0-45°. **(a)** level 1 fractal design; **(b) –** level 2 fractal design; **(c) –** level 3 fractal design; **(d) –** broadband supercell design. The magenta dashed line is a reference to the spectral response at 30° incidence, as carried out experimentally and in matched simulations.

approaching from higher frequencies. This is assumed to be a resonant response of the polyimide. For all other designs (Figure S10b-d), when the absorption frequency is much further away from the secondary absorption curve, its magnitude is diminished. Hence we assume that the absorption of the fractal crosses interfere with the polyimide resonance, which explains the strength of the secondary absorption curve in Figure S10a due to its close proximity to the main fractal absorption curve. This is also seen experimentally in Figure S4a, for the level 1 fractal design (blue curve), where the double peak occurs due to the presence of the polyimide absorption. Also, the broadband simulation (Figure S10d) shows poor performance at all angles, confirmed by experimental results at 30° (shown in Figure S4b), as well as simulated results at both 0° and 30° incidence (shown in Figure S2a and Figure S4b).

References

[1] J. Grant, Y. Ma, S. Saha, A. Khalid, D. R. S. Cumming, *Opt. Lett.* **2011**, *36*, 3476.

[2] J. P. Grant, I. J. H. McCrindle, D. R. S. Cumming, *J. Vis. Exp.* **2012**, e50114.

[3] H.-T. Chen, *Opt. Express* **2012**, *20*, 7165.

[4] Lord Rayleigh, *Proc. R. Soc. London A Math. Phys. Eng. Sci.* **1907**, *79*.

[5] S. Enoch, N. Bonod, *Plasmonics - From Basics to Advanced Topics*, Springer Berlin Heidelberg, Berlin, Heidelberg, **2012**.